Spectrochimica Acta Part A: Molecular and Biomolecular Spectroscopy 171 (2017) 439–448

Contents lists available at ScienceDirect

Spectrochimica Acta Part A: Molecular and Biomolecular Spectroscopy

journal homepage: www.elsevier.com/locate/saa

Adaptive Neuro-Fuzzy Inference system analysis on adsorption studies of Reactive Red 198 from aqueous solution by SBA-15/CTAB composite

Khadijeh Aghajani [a], Habib-Allah Tayebi [b,*]

[a] Department of Computer Engineering, University of Mazandaran, Babolsar, Iran
[b] Department of Textile Engineering, Qaemshahr Branch, Islamic Azad University, Qaemshahr, Iran

ARTICLE INFO

Article history:
Received 23 April 2016
Received in revised form 12 August 2016
Accepted 16 August 2016
Available online 24 August 2016

Keywords:
SBA-15
CTAB
Reactive Red 198
Adsorption study
Adaptive Neuro-Fuzzy Inference systems (ANFIS)

ABSTRACT

In this study, the Mesoporous material SBA-15 were synthesized and then, the surface was modified by the surfactant Cetyltrimethylammoniumbromide (CTAB). Finally, the obtained adsorbent was used in order to remove Reactive Red 198 (RR 198) from aqueous solution. Transmission electron microscope (TEM), Fourier transform infra-red spectroscopy (FTIR), Thermogravimetric analysis (TGA), X-ray diffraction (XRD), and BET were utilized for the purpose of examining the structural characteristics of obtained adsorbent. Parameters affecting the removal of RR 198 such as pH, the amount of adsorbent, and contact time were investigated at various temperatures and were also optimized. The obtained optimized condition is as follows: pH = 2, time = 60 min and adsorbent dose = 1 g/l. Moreover, a predictive model based on ANFIS for predicting the adsorption amount according to the input variables is presented. The presented model can be used for predicting the adsorption rate based on the input variables include temperature, pH, time, dosage, concentration. The error between actual and approximated output confirm the high accuracy of the proposed model in the prediction process. This fact results in cost reduction because prediction can be done without resorting to costly experimental efforts. SBA-15, CTAB, Reactive Red 198, adsorption study, Adaptive Neuro-Fuzzy Inference systems (ANFIS).

1. Introduction

In recent years, the treatment of industrial waste water has gained increasing importance as industrial effluents contain dyes which can result in more pollution of ecosystems [1]. Dyes are used in different industries, especially in textile, leather, pulp, paper, food, plastics, pharmaceutical, cosmetics, and dyestuffs, to name but a few; in particular, textile industries are in the forefront of the use of dyes and the discharge of the largest amount of colored effluent into the environment [2]. Over 70,000 tons of approximately 10,000 different dyes and pigments are used in industries annually worldwide; 20–30% of the dyes are lost in industrial effluents during dyeing and finishing processes due to inefficiencies of the industrial dyeing process [3]. Azo dyes are the largest class of dyes, constituting 60–70% of all dyes produced [4]. Reactive Red 198 (RR 198) is one of the Azo dyes that used for cotton dyeing in textile industry. Removal process of this dye is very difficult due to its high solubility. RR 198 may be toxic to some aquatic organisms, animals and humans because of its carcinogenicity which leads to mutagenic [5].

A wide range of methods have been developed for the removal of dyes and other colored contaminants from industrial waste water including chemical precipitation, electrolysis, aerobic/anaerobic biological degradation, chemical coagulation, membrane filtration, flocculation, photochemical degradation and chemical oxidation. However, these methods suffer from one or more limitations and are unable to adequately reduce dyes concentrations to desired levels [6,7]. Adsorption is one method which is widely used because of its high efficiency, easy operations and low running cost [8]. Various adsorbents such as Fe_3O_4/polyaniline nano composite [9], activated carbon/polyaniline composite [10], eggshell biocomposite dead [11] have been used for the removal of RR 198 from waste water.

In recent years, new hybrid organic- inorganic mesoporous ordered structures are widely investigated as adsorbents for the removal of heavy metal ions, organic dyes, and other organic compounds [12]. SBA-15 is a new kind of ordered mesoporous molecular sieve exhibiting large and uniform pore size distribution, thick amorphous silica walls, large surface area and remarkable thermal and hydrothermal stability [13,14,15]. In addition, the surface of SBA-15 can be readily modified by organic groups that can significantly enhance its adsorption capacity and selectivity [16,17].

Using simulations helps researchers study the effect of various input parameters on the output more easily. This idea results in cost reduction since doing several experiments on all possible combinations of input data is no longer needed [18]. The model which was used in this study is ANFIS. In [19], ANFIS is introduced as a very suitable model in different

* Corresponding author.
E-mail address: tayebi_h@yahoo.com (H.-A. Tayebi).

http://dx.doi.org/10.1016/j.saa.2016.08.025
1386-1425/

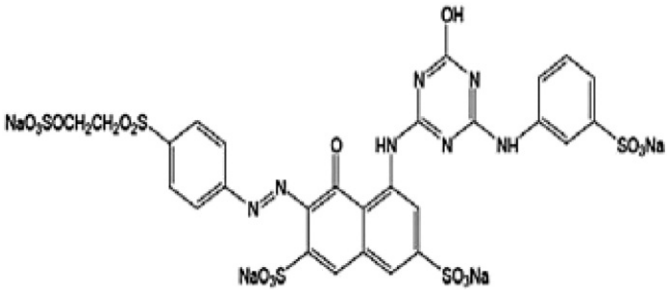

Fig. 1. Chemical structure of RR 198.

environmental engineering aspects. In [20], ANFIS is used for quantitative evaluation of woven fabrics pilling resistance. In [21], it is applied to the prediction of water absorption of geo polymers made from wasted ashes. In [22], ANFIS modelling is used to predict the iodine numbers of activated carbons made from Tabas anthracite. Ghaedi et al. used ANFIS model for modelling the adsorption of 1,3,4-thiadizanole-2, 5-dithiol onto gold nanoparticles-activated carbon [23]. In [24], the authors focused on using ANFIS based-method for the removal of arsenic and chromium from water using a ZEDA hybrid material. In [25], the application of ANFIS modelling in the biodegradation of penicillin-G wastewater using AHR (Anaerobic Hybrid Factor) is discussed. In [26], the effect of annatto dye on Salmonella enteritidis in mayonnaise is predicted using ANFIS model. They also used ANFIS model to predict inactivation of Salmonella enteritidis by ultrasound [27]. In [28], ANFIS model is used to find the best techno economical reactive Blue 19 elimination conditions according to RSM design.

In the present work, SBA-15 was functionalized with Cetyltrimethylammoniumbromide (CTAB) and used as an adsorbent for the removal of reactive Red 198 from aqueous solutions. Also ANFIS model is drived to predict the adsorption rate based on the input variables include temperature, pH, time, dosage, concentration.

2. Experimental

2.1. Materials

Materials such as Pluronic P123 surfactant ($EO_{20}PO_{70}EO_{20}$, $Mw = 5800$), Tetraethylorthosilicate (TEOS, 98%), Hydrochloric acid 37% and sodium hydroxide 99%, Cetyl trimethyl ammonium bromide (CTAB) were supplied from Sigma-Aldrich and Merck. Reactive Red 198 (Reactive Red RB), an anionic dye, was prepared from Dystar (Fig. 1 & Table 1) and was used as received without further purification. A stock solution of RR 198 (1000 mgl^{-1}) was prepared and diluted with the required initial concentration. This dye shows an intense adsorption peak in the visible region at 515 nm. This wave length corresponds to the maximum adsorption peak of RR 198 ($\lambda max = 515$).

2.2. SBA-15 synthesis

According to Zhao et al. [29], Mesoporous SBA-15 was synthesized as follows: 12.5 ml of P123 as surfactant and 375 ml of distilled water as well as 75 ml (0.1 N) of HCl were stirred at 42 °C. After that, 31.5 ml of TEOS, representing the silica source, was added to the homogeneous mixture. The obtained gel was kept in static conditions at 42 °C for 24 h. Next, the temperature was raised to 138 °C and maintained for 24 h. After filtration, the obtained powder was transferred to a furnace for calcinations at 550 °C for 5 h for the purpose of removing existing organics from its pores.

2.3. SBA-15/CTAB synthesis

10 *ml* of Distilled water is poured into a beaker and 0.02 g of CTAB as well as 0.1 g of SBA-15 is added to it; then, all these materials are stirred by a mechanical stirrer for 20 min. Finally, the obtained mixture is filtered by filter papers, washed by distilled water and dried in oven at 70 °C for 5 h.

2.4. Instrumentation

Transmission electron microscope (TEM) image was taken by Hitachi, HF2000. Field emission scanning electron microscope (FESEM) images were obtained using a TESCAN MIRA3 microscope. Low angle X-ray spectra patterns in the range of 0.6â€“9 were determinedby XPERT-PRO40 *kV* spectrometer using Cu Kα radiation ($\lambda = 1.5406$ *A*). FT-IR results were recorded via Shimadzu 4100 Fourier transform infrared spectroscopy. The surface area of SBA-15 and the size of holes before and after the Sited CTAB on SBA-15 were measured by Quanta chrome, Chemo BET 3000 TPR/TPD. Thermo gravimetric analysis (TGA) was done with a Shimadzu TGA50H instrument.

2.5. Adsorption studies

Batch experiments were carried out through contacting different amounts of adsorbent (SBA-15/CTAB) with 100 ml dye (RR 198) solution with different initial concentrations (20–400 ppm) at various pH values (2 − 12) and temperatures of 25, 35 and 45 °C. In order to control pH in the adsorption process, a buffer solution was added. The products were placed in a shaker with 150 rpm velocity for different times (5–120 min). At the end of the process, the adsorbent was separated by centrifuging at 4000 rpm in 30 min. The amount of dye in the solution before and after adsorption process was measured by Jenway 6505 UV–visible spectrophotometer. The quantity of dye adsorbed on SBA-15/CTAB and dye removal precentage (removal efficiency %) were estimated using the following Eq. 1 and 2 [30]:

$$q_e = \frac{(C_0 - C_e)V}{W} \quad (1)$$

where, q_e is the quantity of dye adsorbed on SBA-15/CTAB (mg/g), C_0 and C_e are the initial and final dye concentrations (mg/l), respectively. V is the volume of dye bath (l) and W is the weight of adsorbent (SBA-15/CTAB) (g).

$$R\% = \frac{A_1 - A_2}{A_1} \times 100 \quad (2)$$

where $R\%$ is the removal percentage, A_1 and A_2 are the initial adsorption of dye before and after adsorption process, respectively.

2.6. Modelling using adaptive Neuro-Fuzzy Inference systems (ANFIS)

2.6.1. Fuzzy inference system

Fuzzy modelling is a common approach to modelling the input-output relationship in complex nonlinear systems. Using the fuzzy methodology enables us to define this relationship based on relatively simple calculations on linguistic terms rather than complicated calculations. A general fuzzy system basically includes four parts, namely,

Table 1
Characteristics of RR 198.

Name	CAS number	C.I. number	Formula	Molecular weight	λmax
Reactive Red 198	145017-98-7	18221	$C_{27}H_{18}ClN7O_{15}S_{5.4}Na$	968.21 g/mol	515 nm

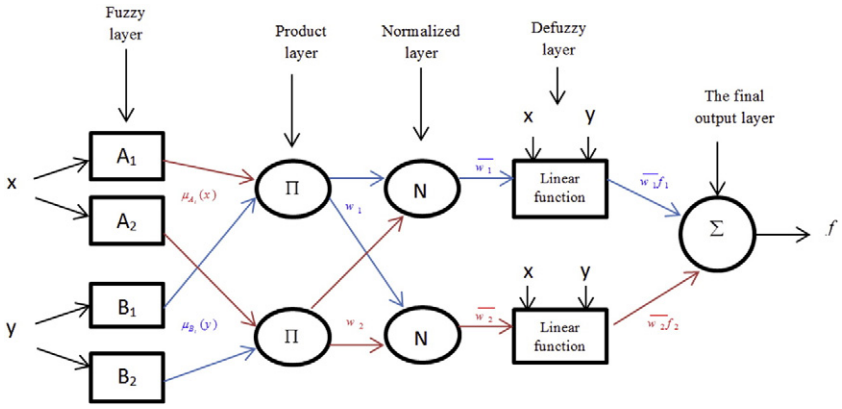

Fig. 2. ANFIS architecture.

fuzzification, fuzzy rule base, fuzzy inference engine and defuzzification [19].

The first component, fuzzifier, represents converting every amount of the input x to a linguistic term; this is done through determining the membership degree which belongs to the range [0 1]. This is performed by applying the membership function tothe input data, $\mu_A(x)$. Gaussian, trapezoidal, sigmoidal and triangular functions are among the common membership functions in fuzzy systems which can be used depending on the nature of the system being studied.

Fuzzy rules include all possible relations and rules between inputs and outputs. This relation is defined in the form of "*if then*" statements. Generally, each fuzzy rule is like "*if x is A then y is B*" where $x \in X$ and *yinY* represent inputs and *A* and *B* stand for linguistic values defined by fuzzy sets on universe of discourse *X* and *Y*.

The *if-part* and *then-part* of fuzzy rules are respectively called antecedent and consequent. The fuzzy inference engine takes into account all rules in the fuzzy rule base and gains the ideal output based on inputs. If the antecedent includes multiple parts, we can use the suitable fuzzy logic operators for mapping the antecedent onto a single number belonging to the range [0 1]. Aggregation is the process by which outputs of different rules are combined in order to make the decision. Maximum (*max*), sum of each rules output (*sum*), the probabilistic OR (*probor*) methods are some commonly used approaches in this section [19].

The last phase in a fuzzy system to gain the ideal output is called defuzzification in which the linguistic results obtained from rules and aggregation are translated into a crisp value. Center of Gravity (COG), mean of maxima (MOM), smallest of maxima (SOM), largest of maxima (LOM), left most maxima, right most maximum and bisector of area are among the most common methods used in this phase [19,31].

FISs are basically divided into two categories, namely, Mamdani and TSK. The outputs of the rules in Mamdani model are fuzzy sets which incorporate linguistic information into the model while in TSK, the output is a linear or a constant function.

2.6.2. ANFIS

ANFIS is a TSK-based fuzzy system which some of its parameters can be learned in order to find an appropriate mapping between the observed inputs and output. The architecture of ANFIS system looks like to Fig. 2 and consists of five layers, namely, a fuzzy layer, a product layer, a normalized layer, a defuzzy layer and a total output layer. The first and the fourth Layers include adaptive nodes and the nodes in the second, the third and the fifth layers are fixed. The term adaptive about the nodes of the first and the fourth layers means that some used parameters in these nodes are determined through training phase. The training process is similar to the training in Artificial Neural networks and it can be done by using appropriate optimization method on minimizing the reconstruction error based on observed data.

In general, the rules used in this system are as follows:

$$If\ (x\ is\ A_1\ and\ y\ is\ B1), then\ f_1 = p_1x + q_1y + r_1 \quad (3)$$

$$If\ (x\ is\ A_2\ and\ y\ is\ B_2), then\ f_2 = p_2x + q_2y + r_2 \quad (4)$$

where *x* and *y* are inputs, A_i's and B_i's represent fuzzy sets and f_i's denote the ideal outputs within the fuzzy regions specified by the appropriate

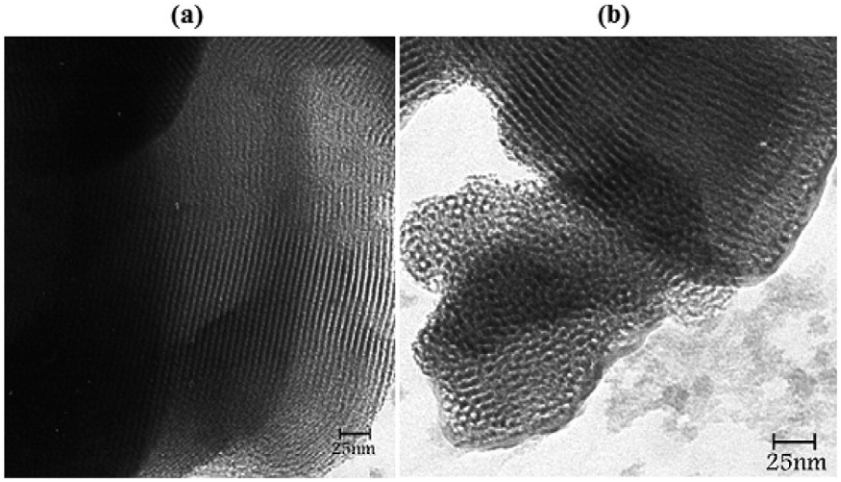

Fig. 3. TEM images of SBA-15 particles before (a) and after (b) modifying with CTAB.

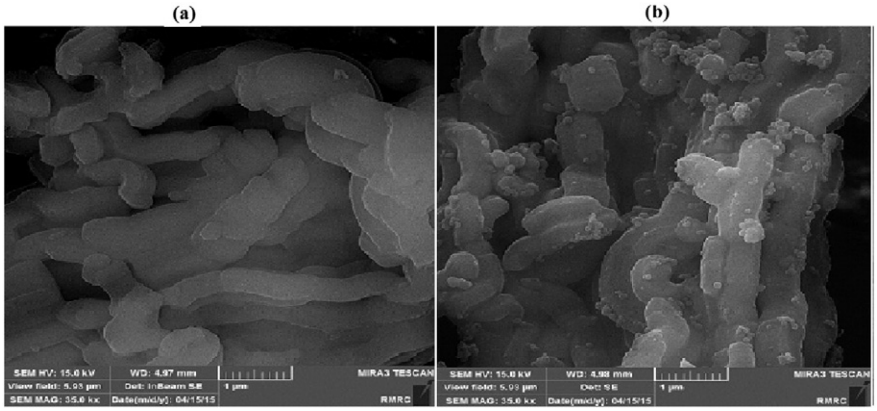

Fig. 4. FESEM images of SBA-15 particles before (a) and after (b) modifying with CTAB.

fuzzy rule. P_i's, q_i's and r_i's are the adjustable parameters that are determined during the training process [19,32,33].

The first layer is the fuzzy layer in which mapping of input variables to corresponding fuzzy membership values is done according to fuzzy membership functions. In the current study, we used Gaussian functions as the membership function whose equation is as follows:

$$\mu_{A_i}(x) = exp\left(-\frac{(x-c_i)}{2\sigma_i^2}\right) \tag{5}$$

where c_i and σ_i^2 represent the mean and variance of the function, respectively. These parameters are called premise parameters and can be updated during training process. The second layer is the product layer which consists of fixed nodes. In this layer, the output of each node is the product of multiplying its inputs. Every w_i denotes the firing strength of each rule. As an example, considering the Fig. 2, one can calculate w_i by the following equation:

$$w_i = \mu_{A_i}(x)\mu_{B_i}(y) \;\; i = 1, 2 \tag{6}$$

The third layer is the normalized layer. In this layer, the output of *i*'th node is calculated according to the ratio of the firing strength of the *i*'th rule to the sum of all rules firing strengths. The output of the node *i* is calculated as follows:

$$\overline{w}_i = \frac{w_i}{w_1 + w_2} \;\; i = 1, 2 \tag{7}$$

The fourth layer is the defuzzification layer. The nodes of this layer are adaptive. In this layer, the output of each node *i* is obtained as:

$$\overline{w}_i f_i = \overline{w}_i(p_i x + q_i y + r_i) \; i = 1, 2 \tag{8}$$

where the linear parameters p_i, q_i and r_i are the ones which are determined during the training process. Finally, the last layer is the total sum of input signals which indicate the final result. The output of this layer can be written as:

$$output = \sum_i \overline{w}_i f_i = \frac{\sum_i w_i f_i}{\sum_i w_i} \tag{9}$$

Table 2
Characteristics of SBA-15 and SBA-15/CTAB samples.

Sample	Surface area (BET) (m^2/g)	Pore diameter (BJH) (nm)	Pore Volume (BJH) (cm^3/g)
SBA-15	743.5	8.2	0.98
SBA-15/CTAB	246.4	4.6	0.44

3. Results and discussion

3.1. Characterization analyses

The structure of produced SBA-15 was characterized by transmission electron microscope (TEM) (Fig. 3). The SBA-15 and SBA-15/CTAB composite TEM images indicate a hexagonal well-ordered mesoporous structure. The pore size diameter of SBA-15 was calculated about 6–8 nm which was not that different from the pore size calculated by BJH (Barrett-Joyner-Halenda) method. BJH method is a pore size distribution determination method, which is typically applied to nitrogen desorption data measured on mesoporous materials [34]. Furthermore, FESEM images of SBA-15 and SBA-15/CTAB are shown in Fig. 4a and b, respectively. According to Fig. 4b and Table 2, functionalization with CTAB took place both inside the pores and outside the SBA-15. Low Angle X-Ray Diffraction patterns of synthesized SBA-15 and SBA-15/CTAB samples are depicted in Fig. 5. These patterns display 3 peaks: one strong peak at 1.035 and two weak peaks at 1.64 and 1.86, respectively, which represent the hexagonal structure of synthesized silicate mesoporous material. The XRD pattern did not vary after the functionalization of SBA-15 with CTAB.

The FTIR spectrums of SBA-15 and SBA-15/CTAB samples in the range 400–4000 cm^{-1} are indicated in Fig. 6. Generally, one attribute of Silicate mesoporous materials is the wide and large bands between 3200 and 3500 cm^{-1} which pertains to Silanol groups and water molecules [35]. The wide adsorption band around 1030 to 1240 cm^{-1} is related to the stretching feature of Si-O-Si [35]. The adsorption band in 1076 cm^{-1} represents the asymmetrical stretching of Si-O-Si. The band in 1608 cm^{-1} shows O—H bonds of water molecules. The symmetrical stretching of Si-O-Si occurs in 760 cm^{-1}. The band 894 cm^{-1} is related to Si-OH and represents Silicate mesoporous materials.

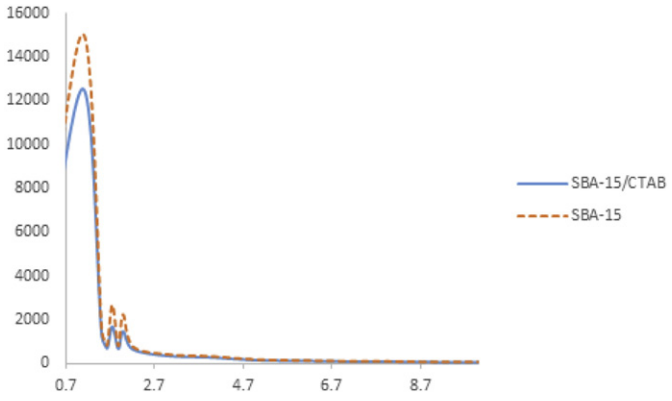

Fig. 5. XRD patterns of SBA-15 and SBA-15/CTAB particles.

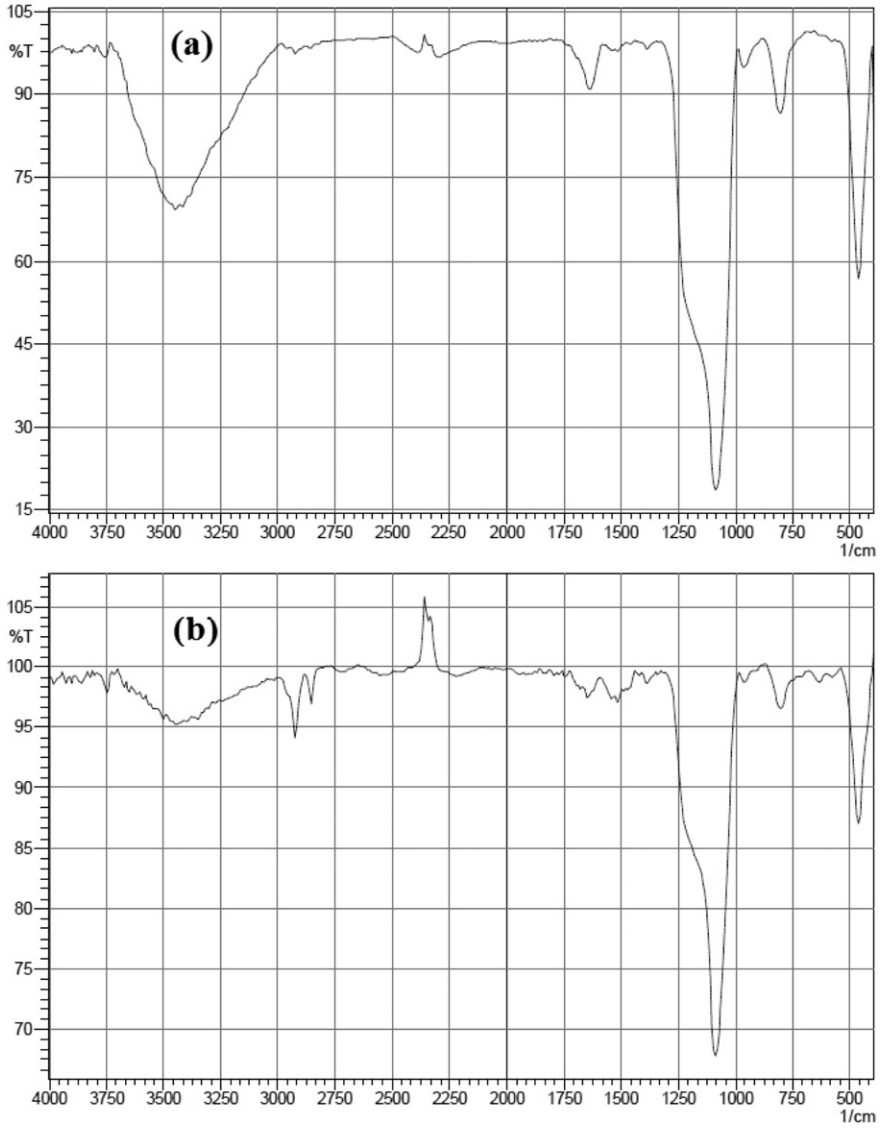

Fig. 6. (a) FTIR spectra of SBA-15 particles before (a) and after (b) modifying with CTAB.

Some of bands in the FTIR pattern related to SBA-15/CTAB, have either disappeared or their peaks have decreased in the presence of SBA-15; it implies the fact that the CTAB molecular chains have lain on SBA-15 particles. In the case of the SBA-15/CTAB sample, peaks at 2940, and 2826 cm^{-1} ascribed to the long alkyl chain of CTAB further prove the presence of CTAB at the surface of SBA-15 [36].

As it is clear from Fig. 7, no destruction is seen on SBA-15 sample when exposed to temperatures of up to 600 °C; this is because of the mineral structure of this compound. However, the sample, the surface of which was modified with CTAB, starts to degrade from 100 °C onward

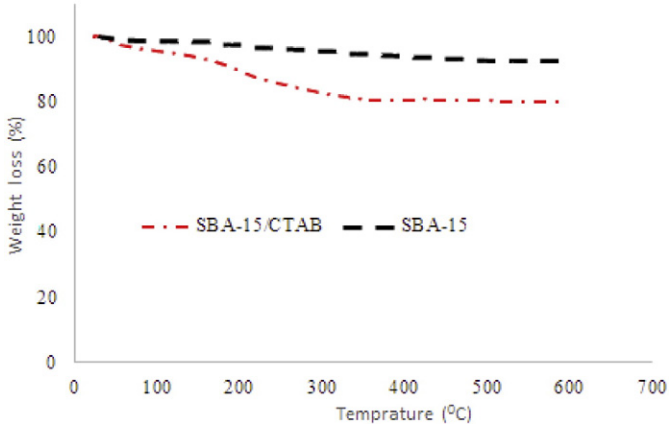

Fig. 7. TGA analysis for SBA-15 and SBA-15/CTAB composite.

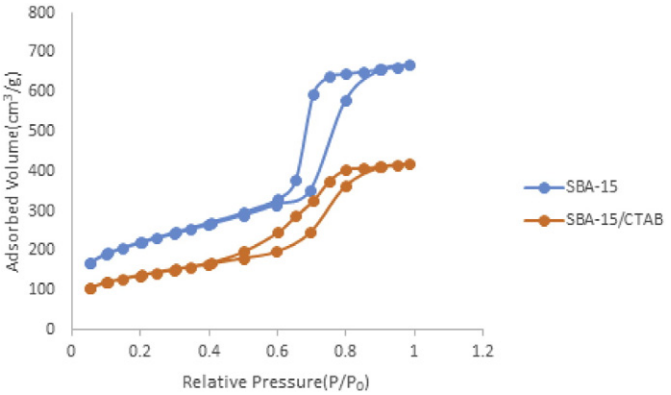

Fig. 8. N_2 adsorption/desorption isotherms of SBA-15 and SBA-15/CTAB.

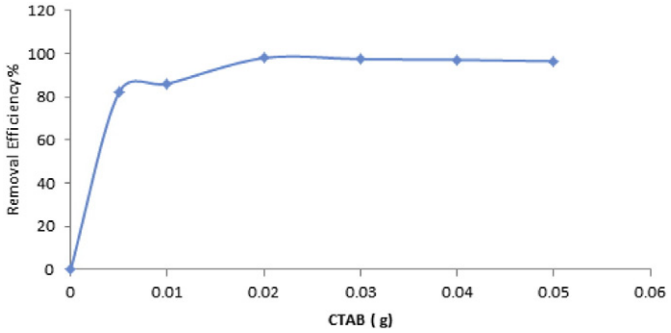

Fig. 9. Effect of CTAB on RR 198 removal (100 ml of 20 mg/l RR 198, time 2 h, $T = 25°$ and SBA-15 = 100 mg).

and this phenomenon continues until a temperature of 350 °C is reached and after that the sample exposed to heat stops degrading; this is because of the thermal destruction of CTAB structure in the SBA-15/CTAB composite. Thus, regarding the obtained data, it can be asserted that the SBA-15/CTAB composite sample is able to stay stable at experiment temperatures which may reach 45 °C, at most.

The N_2 adsorption/desorption isotherms of SBA-15 and SBA15/CTAB are shown in Fig. 8. The SBA-15 sample exhibits isotherm of type IV with a hysteresis loop of type H1 and a sharp increase of adsorbed N_2 at the relative pressure of $P/P_0 = 0.62$, as expected for mesoporous materials [17,35]. In Table 2, the specific BET surface area, pore volume and average pore diameter of SBA-15 and SBA-15/CTAB are summarized. In the case of SBA-15/CTAB, after functionalization of SBA-15 with CTAB, the inflection point of isotherm shifts to lower P/P_0; moreover, the decrease in BET surface area, mesopore volume and pore size of SBA-15/CTAB clearly indicate that the CTAB chains have stuck to channels well.

3.2. Adsorption studies

3.2.1. Effect of CTAB

The reported values in this Section represent the optimum conditions for an experiment in which a fixed 0.1 g of SBA-15 is used and the amount of CTAB varies between 0.005 and 0.05 g. The adsorbents resulted from this experiment were used to remove a dye solution with a concentration of 20 ppm. As it can be seen in Fig. 9, the highest percentage of dye removal is resulted when a 0.02 g of CTAB is used. Thus, this adsorbent, i.e. the composite prepared from 0.1 g of SBA-15 and 0.02 g of CTAB, was used for future experiments.

3.2.2. Effect of pH

In the adsorption process, the pH of solution is one of the most important parameters which controls the adsorption of dye molecules in the adsorption sites. Therefore, a study is carried out in order to optimize pH while other parameters such as the amount of adsorbent (SBA-15/CTAB), dye concentration, and temperature are fixed. Fig. 10 indicates the effect of pH on dye removal efficiency as a function of pH. The primary dye concentration was 20 mg/l and the adsorbent amount equaled 0.1 g. Dye adsorption increases while pH reaches 2 and the maximum adsorption occurs in this case; as in the acidic pH, more protonation of the adsorbent surface is probable which results in higher dye adsorption.

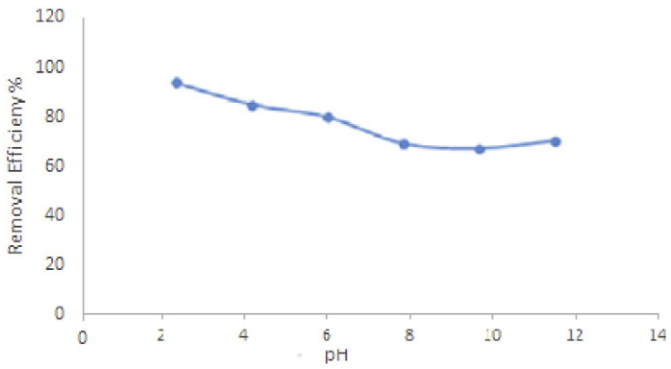

Fig. 10. Effect of pH on RR 198 removal (100 ml of 20 mg/l RR 198, time 2 h, $T = 25$ °C and dosage = 100 mg).

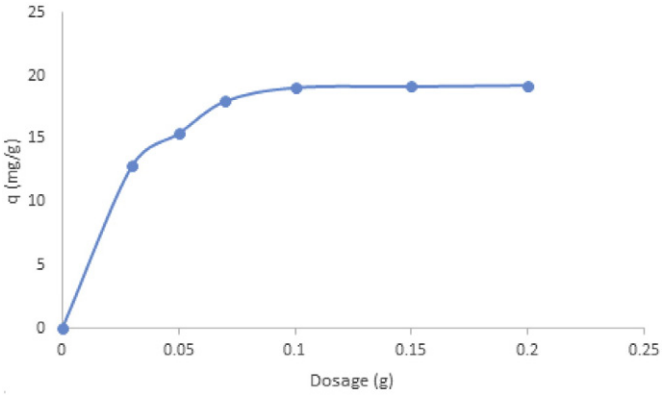

Fig. 11. Effect of dosage on RR 198 removal (100 ml of 20 mg/l RR 198, time 2 h, $T = 25$ °C and pH = 2).

3.2.3. Effect of adsorbent dosage

The effect of adsorbent amount on dye removal was examined in pH = 2 with 100 ml of the dye solution (20 mg/l) and it was displayed in the Fig. 11. The figure shows that the percentage of dye removal depends on increasing the adsorbent amount and it is raised by the increase of adsorbent to the point that it reaches the highest amount 99% while the adsorbent is 100 mg; the reason is as the adsorbent amount rises, the adsorbing sites increase and these sites are more likely to adsorb the dye. However, by increasing the adsorbent amount up to 0.1 g, the adsorption amount was not raised due to the accumulation of adsorbent particles. Therefore, 1 g/l of adsorbent (SBA-15/CTAB) is the optimum adsorbent amount.

3.2.4. Effect of contact time and temperature

In this section, dye (RR 198) adsorption by the adsorbent (SBA-15/CTAB) was investigated as a function of contact time and the results were displayed in Fig. 12. It is observed that dye adsorption is fast at the beginning and after 60 min it is balanced. At the beginning of the process, changes in adsorption amount happen fast because more adsorbing sites are available; and after 60 min, the process reaches balance and the adsorbing sites are saturated.

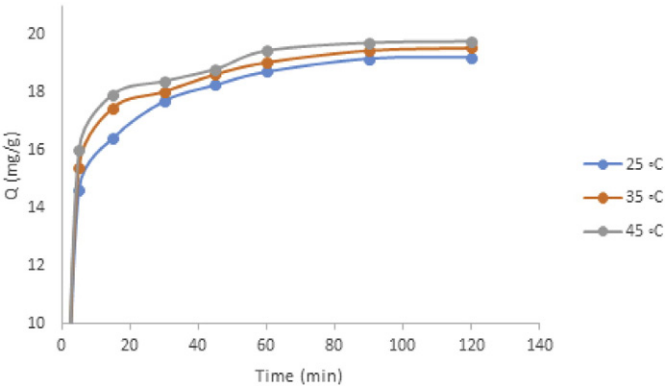

Fig. 12. Effect of time on RR 198 removal (100 ml of 20 mg/l RR 198, dosage = 100 mg, $T = 25$ °C and pH = 2).

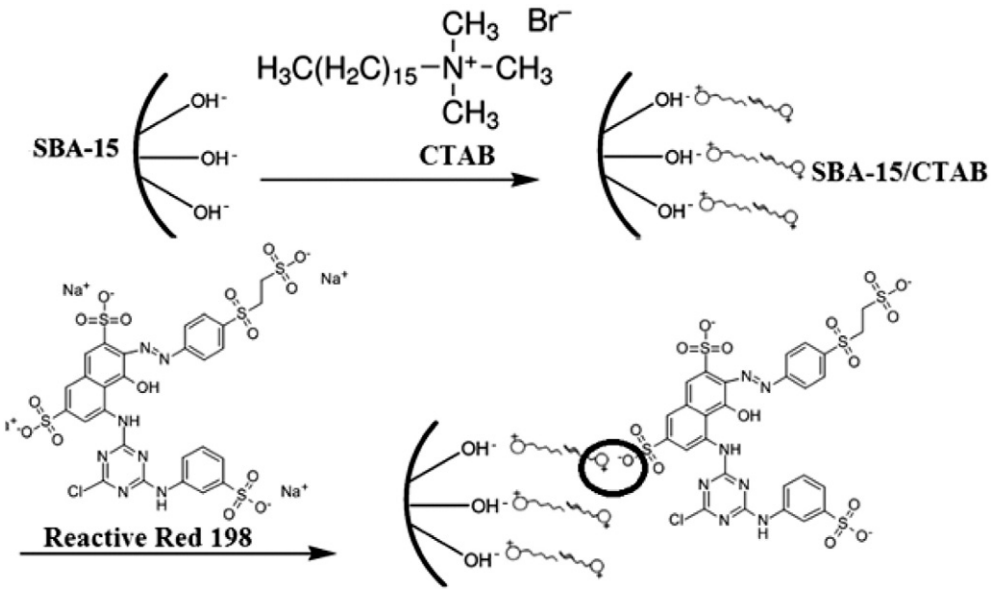

Fig. 13. Schematic illustration of SBA-15 surface modification process with CTAB and dye adsorption mechanism.

As it is seen in Fig. 12, the adsorption amount was increased by raising the temperature which implies that the adsorption process is endothermic.

3.2.5. Adsorption mechanism

The active surface area of SBA-15 is very large (743.5 m^2/g). Therefore, the contact surface between CTAB and SBA-15 will also be so large and this will lead to the occurrence of many interactions. Considering the neutral pH of the process environment, the amount electro-kinetic charge of SBA-15 is negative (−35 mV) [37]. As it can be seen in Fig. 13, CTAB possesses a positive charge and settles on the Hydroxyl groups of SBA-15 which have negative charges, and by contacting another CTAB molecule, adhered to the dye molecule through its sulfonic group, results in the adsorption of the dye.

3.3. Implementation of ANFIS model

The implementation of this section was done in Matlab. The creation and training of FIS are done using a fuzzy clustering-based method. In clustering-based methods, after determining the clusters, the membership functions and finally rules related to each cluster are identified through the training procedure. In this study, an FCM-based method was used for clustering. The training and testing processes were carried out according to observed data. Each data record includes inputs and corresponding output values. Here, the output is the amount of adsorption and the input includes variables such as pH, dosage, time, concentration and temperature. 70% of data was used for training and the remaining 30% was used for evaluating the trained model. The training data are randomly chosen from 70% of the whole data.

As it is known, one of the required parameters in FCM-based clustering is the number of clusters. This number was considered 17 in

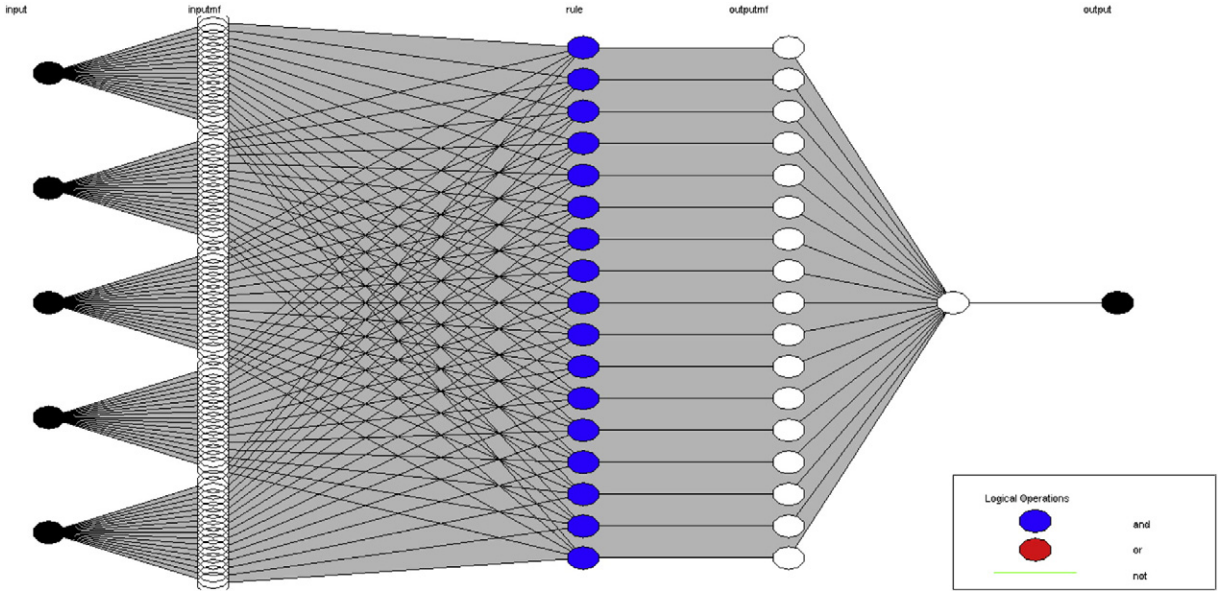

Fig. 14. The obtained structure of the ANFIS for the given 5 inputs.

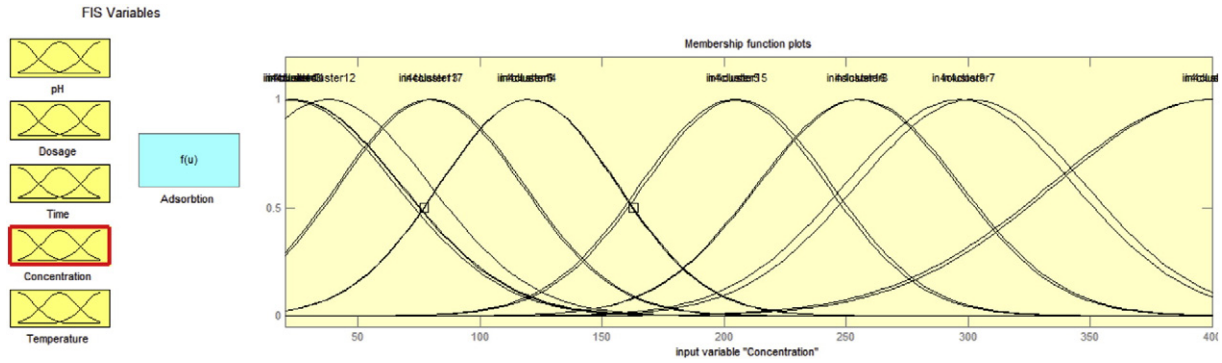

Fig. 15. The adjusted membership functions for concentration.

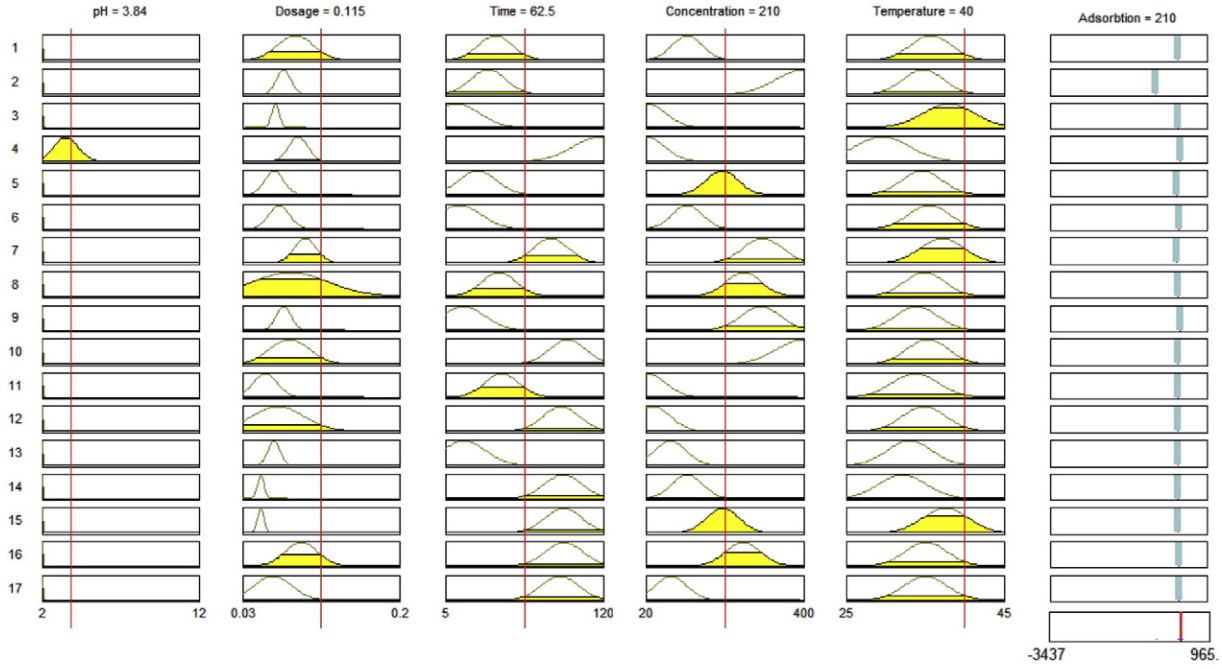

Fig. 16. The application of the obtained ANFIS model.

our study based on trial and error. After carrying out the training process, we obtained the construction of an ANFIS model shown in Fig. 14.

As it was mentioned before, the parameters of the membership functions for each input are determined during the training process. As an example, in the Fig. 15, a membership function of the fourth input, concentration, is displayed. The application of ANFIS system is also depicted in Fig. 16. How this system operates in different layers can be observed in this figure.

Some surface plots of output based on two arbitrary inputs are also displayed in Fig. 17.

Two criterions, namely, CC (Correlation Coefficient) and RMSE (Root Mean Square Error) were used for system evaluation. CC stands for the correlation between the observed and the obtained outputs predicted by the model. In training and testing data, this parameter is calculated through the following equation:

$$CC = \frac{\sum_i (x_i - \overline{x_i})(y_i - \overline{y_i})}{\sqrt{\sum_i (x_i - \overline{x_i})^2 \sum_i (y_i - \overline{y_i})^2}} \tag{10}$$

where x_i and y_i are the observed and the predicted values, respectively. The variation patterns of observed and predicted data in batch process in training and testing phase are presented in Fig. 10. The values of CC are shown above every image in Fig. 10.

Another parameter which is used for evaluating the model is RMSE that is calculated through the following equation in testing and training data.

$$RMSE = \sqrt{\frac{\sum_i (x_i - y_i)^2}{N}} \tag{11}$$

where N is the number of data points. The observed and the predicted values for testing and training data and the amount of RMSE value in each set are shown in Fig. 19. The images in Fig. 19 and the obtained parameters properly imply the accuracy of the trained model in predicting the adsorption amount based on its inputs.

As it was already explained, training and testing data are chosen randomly (Training data are randomly chosen first and then, the rest of the data are devoted to testing). Undoubtedly, every random selection results in systems with minor differences and different evaluative parameters. The results of systems displayed in Figs. 18 and 19 are related to carrying out one experiment. In order to investigate the proposed system more realistically, we performed training and testing 50 times

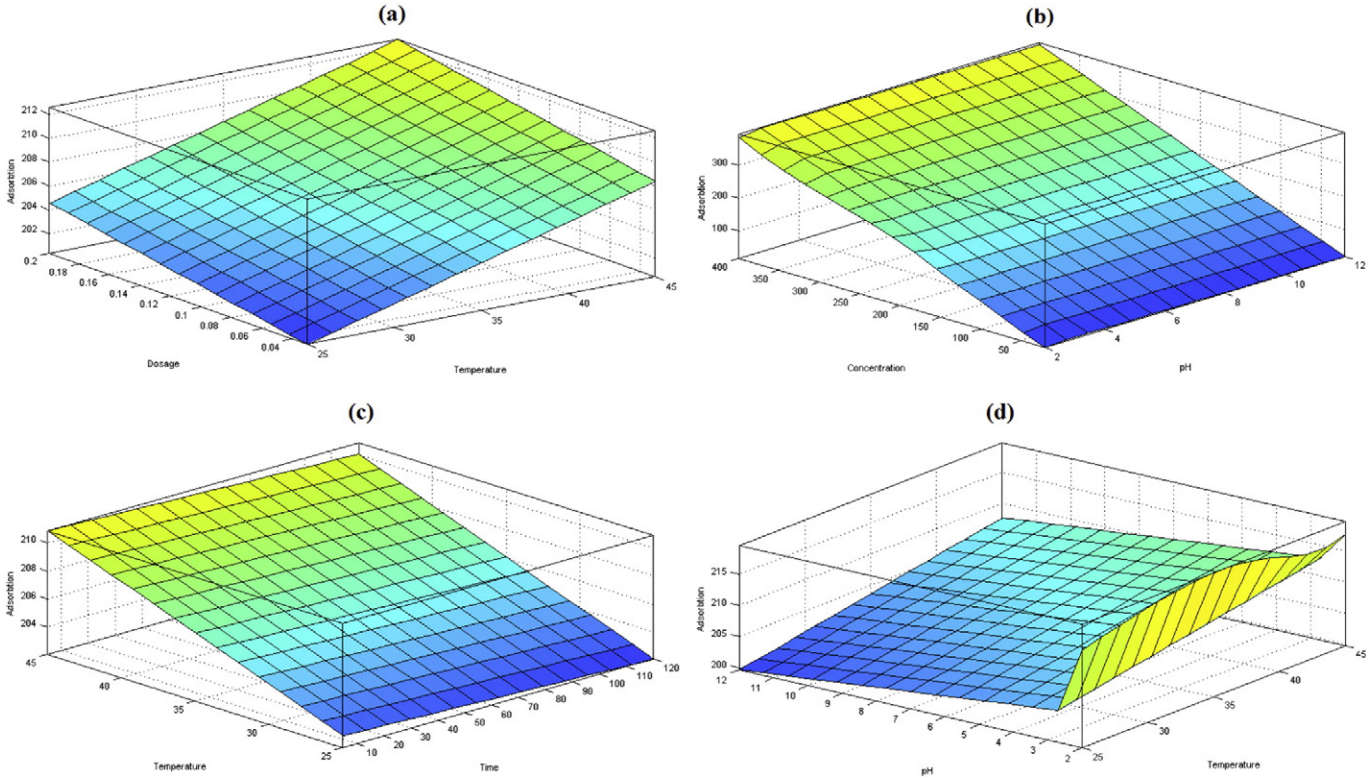

Fig. 17. Surface plots for batch studies (a) dosage versus temperature, (b) concentration versus pH, (c) temperature versus time and (e) pH versus temperature.

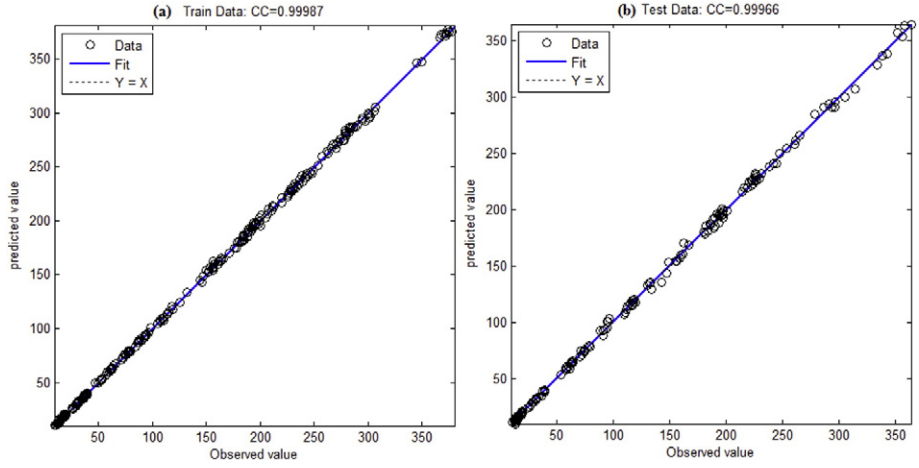

Fig. 18. (a), (b) The correlation plot of observed versus predicted values in training and testing data, respectively.

and evaluative parameters were obtained per experiment (in each run the training and testing data are chosen randomly). Table 3 depicts the average and standard deviation of parameters RMSE and CC obtained after doing all the experiments. The numbers of this table confirm the strength of this model in predicting the results.

4. Conclusion

In this work, SBA-15 was synthesized and modified with CTAB. According to the obtained results, SBA-15/CTAB adsorbent had high efficiency for RR 198 removal from aqueous media. Optimal conditions of RR 198 removal was obtained at pH = 2, contact time of 60 min and dosage of 1 g/l. It has shown that ANFIS model can be used to predict the adsorption rate based on the input variables include temperature, pH, time, dosage, concentration. In creating and training the FIS, FCM-clustering method is used. It is found that ANFIS model with Gaussian type MFs for all input variables and linear relation for its output gives us a very good predictive model. To validate the model, the predicted values are compared to the measured ones. Two criterions, CC and RMSE, are used for comparison. The high amount of CC (approximately 0.9997) and the low amount of RMSE (approximately 2.3) in testing and training data represent the high efficiency of the predictive model.

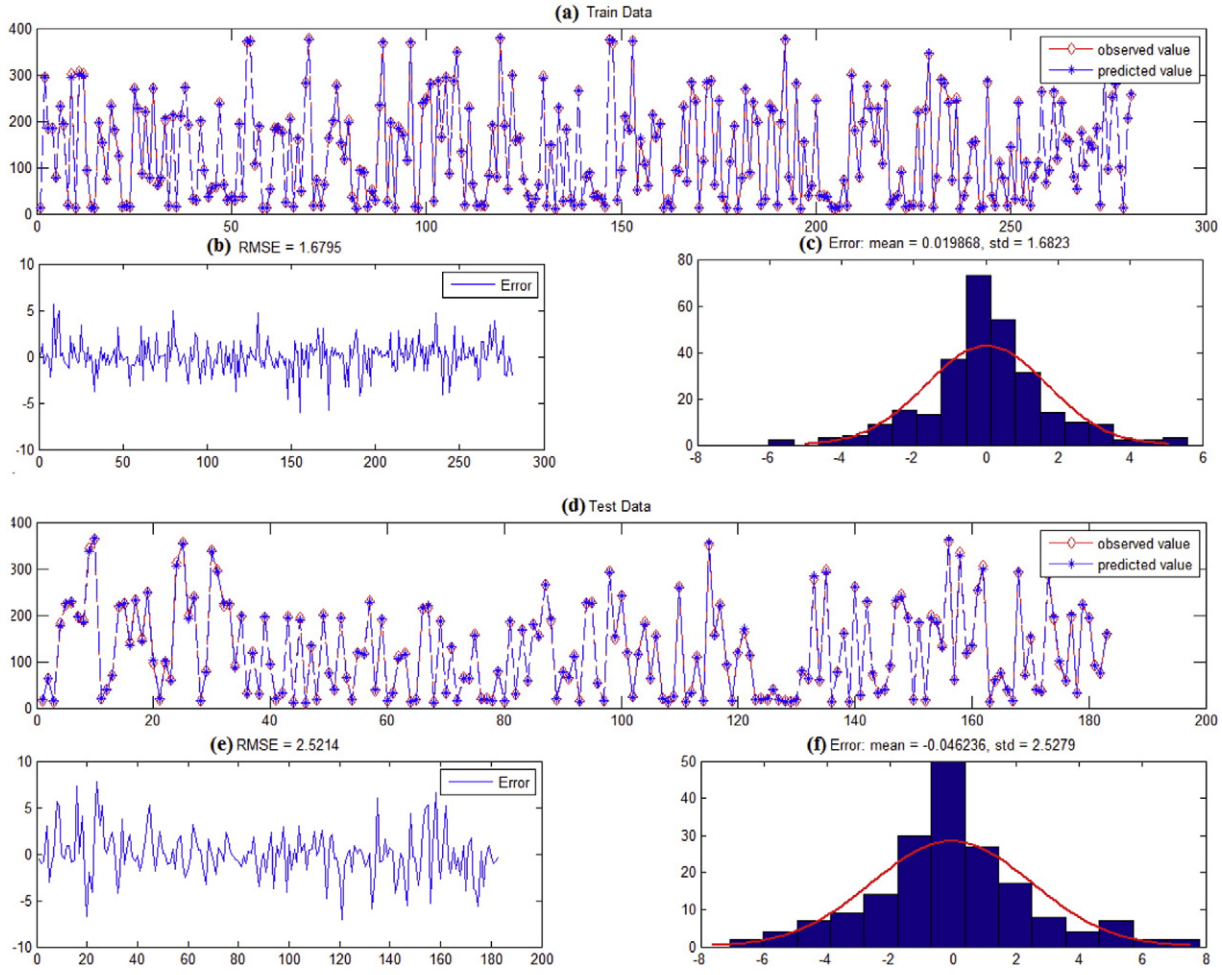

Fig. 19. Evaluating the prediction model in training and testing data. (a), (d) Distribusion of observed and predicted values in training and testing data, respectively. (b), (e) Error amount between the observed and the predicted values in training and testing data, respectively. (c), (f) The histograms of errors in training and testing data, respectively.

Table 3
Performance evaluation of the model in various experiments. Mean and standard deviation of the CC and RMSE parameters obtained after 50 runs in training and testing data.

	CC		RMSE	
	mean	std	mean	std
Training data	0.9997	$0.70*10^{-4}$	1.91	0.318
Testing data	0.9995	$0.94*10^{-4}$	2.81	0.268

References

[1] M. Anbia, S.A. Hariri, S.N. Ashrafizadeh, Appl. Surf. Sci. 256 (2010) 3228–3233.
[2] E. Forgacs, T. Cserhati, G. Oros, Environ. Int. 30 (2004) 953–971.
[3] I.A.W. Tan, A.L. Ahmad, B.H. Hameed, J. Hazard. Mater. 154 (2008) 337–346.
[4] C. Maximo, M.T.P. Amorim, M.C. Ferreira, Enzym. Microb. Technol. 32 (2003) 145–151.
[5] B. Manu, S. Chaudhari, Process Biochem. 38 (2003) 1213–1221.
[6] N. Dizge, C. Aydiner, E. Demirbas, M. Kobya, S. Kara, J. Hazard. Mater. 150 (2008) 737–746.
[7] P. Canizares, Pablo, F. Martinez, C. Jimenez, J. Lobato, M.A. Rodrigo, Environ. Sci. Technol. 40 (2006) 6418–6424.
[8] V.K. Gupta, A. Mittal, L. Krishnan, V. Gajbe, Sep. Purif. Technol. 40 (2004) 87–96.
[9] H.A. Tayebi, Z. Dalirandeh, A. Shokuhi Rad, A. Mirabi, E. Binaeian, Desalin. Water Treat. 1-13 (2016).
[10] D. Zareyee, H. Tayebi, S.H. Javadi, Iran. Org. Chem. 4 (2012) 799–802.
[11] M.F. Elkady, A.M. Ibrahim, M.M. Abd El-Latif, Desalination 278 (2011) 412–423.
[12] M. Mureseanu, A. Reiss, I. Stefanescu, E. David, V. Parvulescu, G. Renard, V. Hulea, Chemosphere 73 (2008) 1499–1504.
[13] A. Katiyar, S.H. Yadav, P.G. Smirniotis, N.G. Pinto, J. Chromatogr. A 1122 (2006) 13–20.
[14] K. De Witte, P. Cool, I. De Witte, L. Ruys, J. Rao, G. Van Tendeloo, E.F. Vansant, J. Nanosci. Nanotechnol. 7 (2007) 2511–2515.
[15] S.E. Rankin, B. Tan, H.J. Lehmler, K.P. Hindman, B.L. Knutson, Microporous Mesoporous Mater. 73 (2004) 197–202.
[16] J.H. Yim, D.I. Kim, J.A. Bae, Y.K. Park, J.H. Park, J.K. Jeon, S.H. Park, J. Song, S.S. Kim, J. Nanosci. Nanotechnol. 11 (2011) 1714–1717.
[17] M. Shafiabadi, A. Dashti, H.A. Tayebi, Synth. Met. 212 (2016) 154–160.
[18] M. Ghaedi, E. Shojaeipour, A.M. Ghaedi, R. Sahraei, Spectrochim. Acta A 142 (2015) 135–149.
[19] K. Yetilmezsoy, B. Ozkaya, M. Cakmakci, Neural Netw. World 21 (2011) 193.
[20] M. Eldessouki, M. Hassan, Expert Syst. Appl. 42 (2015) 2098–2113.
[21] A. Nazari, S.R. Ali, J. Non-Cryst. Solids 358 (2012) 40–46.
[22] S. Rashidi, A. Ahmadpour, N. Jahanshahi, M.J.D. Mahboub, H. Rashidi, Sep. Sci. Technol. 50 (2015) 110–120.
[23] M. Ghaedi, R. Hosaininia, A.M. Ghaedi, A. Vafaei, F. Taghizadeh, Spectrochim. Acta A 131 (2014) 606–614.
[24] S. Mandal, S.S. Mahapatra, R.K. Patel., J. Water Process Eng. 5 (2015) 58–75.
[25] P. Mullai, S. Arulselvi, H.-H. Ngo, P.L. Sabarathinam, Bioresour. Technol. 102 (2011) 5492–5497.
[26] M. Yolmeh, M.B.H. Najafi, F. Salehi, Bioresour. Technol. 67 (2014) 36–40.
[27] B. Soleimanzadeh, L. Hemati, M. Yolmeh, F. Salehi, J. Food Saf. 35 (2015) 220–226.
[28] M. Taheri, M.R.A. Moghaddam, M. Arami, J. Environ. Manage. 128 (2013) 798–806.
[29] D. Zhao, Q. Huo, J. Feng, B.F. Chmelka, G.D. Stucky, J. Am. Chem. Soc. 120 (1998) 6024–6036.
[30] H.A. Tayebi, M.E. Yazdanshenas, A. Rashidi, R. Khajavi, M. Montazer, J. Eng, Fiber Fabr. 10 (2015) 97–108.
[31] M. Ghaedi, A.M. Ghaedi, F. Abdi, M. Roosta, A. Vafaei, A. Asghari, Ecotoxicol. Environ. Saf. 96 (2013) 110–117.
[32] M.Y. Chen, Inf. Sci. 220 (2013) 180–195.
[33] J.S. Jang, IEEE Trans. Syst. Man Cybern. 23 (1993) 665–685.
[34] E.P. Barrett, L.G. Joyner, P.P. Halenda, J. Am, Chem. Soc. 73 (1951) 373380.6.
[35] Q. Cheng, V. Pavlinek, A. Lengalova, C. Li, Y. He, P. Saha, Microporous Mesoporous Mater. 93 (2006) 263–269.
[36] A. Barhoum, H. Rahier, R.E. Abou-Zaied, M. Rehan, T. Dufour, G. Hill, A. Dufresne, ACS Appl. Mater. Interfaces 6 (2014) 2734–2744.
[37] J.M. Rosenholm, M. Lindn, J. Controlled Release 128 (2008) 157–164.